Green's function approach for a dynamical study of transport in metal/organic/metal structures

Z. G. Yu, D. L. Smith, A. Saxena, and A. R. Bishop
Los Alamos National Laboratory, Los Alamos, New Mexico 87545
(Received 5 November 1998; revised manuscript received 15 January 1999)

We develop an efficient Green's function formalism to study transport in organic tunneling devices. We find a crossover behavior of the transport from free-electron-like to polaronlike as the ratio between the electronic and organic lattice vibration time scales is varied. If the electronic time scale is fast compared to the lattice vibration time scale, the lattice motion lags behind the incoming wave packet and the transmission is similar to that in a static case where the lattice is frozen. In the opposite limit, the lattice follows the electron and the first transmission peak shifts from the conduction-band edge toward the self-trapped polaron level. We investigate the transmission coefficient, the transfer of energy between the incident electron and the lattice, and the time evolution of the electron energy distribution function as the ratio of these time scales is changed. To simulate lattice fluctuations we study a preexisting lattice distortion and find enhanced subgap transmission. Our results are important for understanding electrical injection in polymer light-emitting diodes and other organic-based electronic device structures, and electrical transport in molecular wires. [S0163-1829(99)04223-X]

I. INTRODUCTION

Recently, conjugated organic materials have attracted much theoretical and experimental interest both because of the novel physics that occurs in these materials and because of the technological potential of electronic devices fabricated from them.[1–14] In organic-based electronic devices such as polymer light-emitting diodes (PLED's), metal contacts are attached to the conjugated organic material for electron injection. This injection process plays an important role in the operation of organic electronic devices and is not currently well understood. Self-assembled monolayers chemically bonded to the metal contacts have been used to control the injection properties in these devices.[5] Self-assembled monolayers with dipole moments were used to change the energy barrier to injection. The electrons conduct through the molecules making up the self-assembled monolayer which act as an array of molecular wires. The electrical transport in individual molecular wires either contacted by metal pads or by a scanning tunnel microscope tip and a back metal contact[7–10] is a closely related subject also of current interest. A common characteristic of these structures is that an electron is transferred from a metal, where the electron-lattice coupling is weak, to a conjugated organic material, where the electron-lattice coupling is very strong. In conjugated organics, because of the strong electron-lattice coupling, the primary single-particle excitation is not the free electron but the self-trapped polaron, in which a lattice distortion is localized around the electron.[15] Therefore in organic injection structures, polaron formation and lattice fluctuation effects may play a significant role in the electrical transport.[16,17] As a specific structure to investigate transport from a weak electron-lattice coupling material to a strong one, we consider metal/organic/metal tunnel structures. We construct an electron wave packet in one of the metal leads, allow it to impact on the organic region, and study the dynamics of the transport of the wave packet.

Many current studies of electrical injection in organic structures borrow ideas developed for inorganic semiconductor tunneling structures.[18–20] In the description of electrical transport in molecular wires, for example, the organic molecular chain is often treated as an inorganic semiconductor with a rigid lattice.[11–13] Dynamical wave packet evolution approaches have been used to study the transport in inorganic devices.[21] Because of the different nature of interactions in the organic and inorganic materials, it is difficult to extend these approaches to the metal/organic/metal structures, which requires the self-consistent solution of the wave packet plus the lattice problem. Because of the strong electron-lattice interaction and the importance of the lattice configuration to the electronic motion, electrical transport in these structures is an intrinsically dynamical problem, i.e., the evolution of both the incoming electron and organic lattice must be determined self-consistently. Therefore a static study may not be sufficient to obtain a complete understanding of electrical transport in these organic structures. However, due to the complexity and numerical intensity of the dynamical calculations, only static studies have been carried out to date.[11–14]

There have been several studies on the soliton/polaron dynamics in a homogeneous finite polymer chain.[22–27] In these studies, dynamical evolution approaches were developed, which successfully addressed interesting bulk transport questions such as how a preformed soliton/polaron moves in the presence of an external field and how an optically generated electronic excitation evolves into a stable polaron/soliton. The system we study here is intrinsically inhomogeneous in that it consists of two kinds of material regions, weak-coupling metal leads and the strong-coupling conjugated organic material. We are interested in the reflection and transmission coefficients for an electron wave packet incident from the metal, the wave-packet behavior in the lattice (free-electron vs polaron), and lattice fluctuation effects on the electronic transmission. Infinite metal leads are required in order to eliminate the spurious multiscattering that would result from the boundary of a finite system. Be-

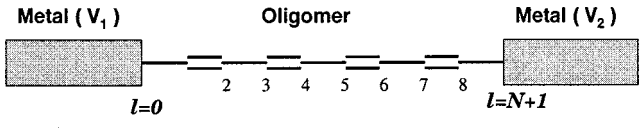

FIG. 1. Schematic diagram showing metal and oligomer sites in a chain for $N=8$.

cause of the infinite metal leads the energy spectrum is continuous rather than discrete as is the case for a finite system. Because we are considering an infinite system with a continuous energy spectrum, the previous mathematical approaches used to describe the dynamics for a finite homogeneous polymer are not suitable to study the transport in the metal/organic/metal structure. We therefore develop a Green's function formalism to study electrical transport in the metal/organic/metal structures. The formalism takes into account the infinite metal leads, possible electrical bias, impurities, the possibility of asymmetric metal contacts, and extrinsic (*cis*-like conformation) contribution to the electronic energy gap, and can be readily extended to other organic structures and device configurations. Using this Green's function formalism, we find that the electron transport behavior indeed depends on the ratio between electronic and lattice time scales. For fixed electronic structure, a crossover behavior from free-electron to polaronlike transport is found with increasing phonon frequency. In the former, the lattice lags behind the incoming wave packet and the transmission is close to that of the static case; whereas, in the latter, the lattice follows the injected electron forming a lattice distortion cloud around the electron, and the transmission peak shifts toward a polaron level in the oligomer.

The paper is organized as follows. In Sec. II, we present the details of the Green's function formalism. Section III contains results on the time evolution of a wave packet as it traverses the oligomer, electronic transmission as a function of energy, energy distribution between the wave packet and the lattice as a function of time, and charge density in the oligomer as a function of time. In Sec. IV, we summarize our conclusions.

II. MODEL AND FORMALISM

We consider a one-dimensional structure in which an oligomer chain is sandwiched between two metal contacts. The metals attached to the oligomer may be different and there may be a bias between the metal leads (Fig. 1). To avoid the spurious multiscattering that would result from the boundary in a finite system, we take infinitely long metal leads. Because the system is infinite the energy spectrum is continuous.

The Hamiltonian consists of four parts:

$$H=H^L_{\rm met}+H^R_{\rm met}+H_{\rm oli}+H_{\rm int}. \tag{1}$$

We describe the metals by using a one-dimensional (1D) tight-binding model, for the left lead,

$$H^L_{\rm met}=-t_0\sum_{l=-\infty}^{-1}(c_l^\dagger c_{l+1}+{\rm H.c.})+V_1\sum_{l=-\infty}^{0}c_l^\dagger c_l, \tag{2}$$

and for the right lead,

$$H^R_{\rm met}=-t_0\sum_{l=N+1}^{\infty}(c_l^\dagger c_{l+1}+{\rm H.c.})+V_2\sum_{l=N+1}^{\infty}c_l^\dagger c_l, \tag{3}$$

where c_l ($c_l^\dagger$) annihilates (creates) an electron at site l, and V_1 and V_2 are the electrostatic potentials of the left lead and the right lead, respectively. The oligomer is described by using the Su-Schrieffer-Heeger (SSH) model:[15]

$$H_{\rm oli}=H^e_{\rm oli}+H_{\rm latt}, \tag{4}$$

$$H^e_{\rm oli}=-\sum_{l=1}^{N-1}\{[t-\alpha(u_{l+1}-u_l)](c_l^\dagger c_{l+1}+{\rm H.c.})+V_l c_l^\dagger c_l\}, \tag{5}$$

$$H_{\rm latt}=\frac{K}{2}\sum_{l=1}^{N-1}\Delta_l^2+\sum_{l=2}^{N-1}\frac{p_l^2}{2M}. \tag{6}$$

Here u_l is the lattice displacement of site l, $\Delta_l=u_{l+1}-u_l$, α the electron-lattice coupling, K the spring constant of the oligomer, and M the mass of the oligomer atom. The term $V_l c_l^\dagger c_l$ represents the site energy change due to a possible electrical bias. This term can also be used to simulate disorder due to impurities. The coupling between the oligomer and the metals is described by hopping at the ends of the oligomer:

$$H_{\rm int}=-t_1(c_0^\dagger c_1+c_N^\dagger c_{N+1}+{\rm H.c.}). \tag{7}$$

The left metal lead extends from $l=-\infty$ to $l=0$ and the right metal lead extends from $l=N+1$ to $l=\infty$. The oligomer extends from $l=1$ to $l=N$. The position of the sites $l=1$ and $l=N$ are fixed and the position of the other $N-2$ sites in the oligomer can vary. The integer N is even.

We explicitly include the valence electrons in the oligomer and the electrons below the Fermi energy in the metals. In the ground state the oligomer is dimerized and polarons are the primary single-particle excitations. In the polaron, the charge is localized and surrounded by a lattice distortion.

We neglect electron-electron interactions and assume the energy of the incoming wave packet is far above the Fermi energy so that all the states of the outgoing electron are unoccupied. We consider both the metal and the metal/oligomer contact as ideal one-dimensional structure. The transmission features depend weakly on the detailed structure of the metal/contacts and the dimensionality of the metals. In our static study, we systematically studied 1D/2D/3D structures and found that they have similar transport features.[14]

We regard the decoupled metals and oligomer to be described by the unperturbed Hamiltonian

$$H_0=H^L_{\rm met}+H^R_{\rm met}+H^e_{\rm oli}. \tag{8}$$

The Green's function of H_0 is calculated from

$$\tilde{G}^0_{ll'}(E)=\sum_i\frac{\langle l|\phi_i\rangle\langle\phi_i|l'\rangle}{E-E_i+i0^+}. \tag{9}$$

Because the oligomer and the two metal contacts are decoupled in H_0 this Green's function for each of these regions can be calculated separately. Since the oligomer is small, $|\phi_i\rangle$ and E_i can be obtained by direct diagonalization of a

small matrix. For the left metal, because of the boundary condition, the eigenfunctions are

$$|\phi_k\rangle = \frac{1}{\sqrt{\mathcal{N}}} \sum_l [e^{ikl} - e^{-ik(l-2)}]|l\rangle. \tag{10}$$

Thus the Green's function at the left metal is $(l,l'<0)$,

$$\tilde{G}^0_{ll'}(E) = \frac{1}{2\pi}\int_{-\pi}^{\pi} dk \frac{e^{ik(l-l')} - e^{ik(l+l'-2)}}{E + i0^+ - V_1 + 2t_0 \cos k}. \tag{11}$$

Similarly, at the right metal $(l,l'>N)$,

$$\tilde{G}^0_{ll'}(E) = \frac{1}{2\pi}\int_{-\pi}^{\pi} dk \frac{e^{ik(l-l')} - e^{ik(l+l'-2N)}}{E + i0^+ - V_2 + 2t_0 \cos k}. \tag{12}$$

Since our model includes two semi-infinite metal leads, the energy spectrum of the system is continuous. We calculate the energy change of the system after turning on the coupling between the metals and the oligomer by integrating over the whole energy spectrum,

$$\delta\mathcal{E} = \int dE E \, \delta\rho(E), \tag{13}$$

where $\delta\rho(E)$ is the change in the density of states that results from turning on the coupling. Using t-matrix theory,[28] it can be written as

$$\delta\rho(E) = \frac{-1}{\pi} \mathrm{Im} \frac{d}{dE} \ln D(E), \tag{14}$$

where

$$D(E) = \det[1 - \tilde{\mathcal{G}}^0(E) H_{\mathrm{int}}]. \tag{15}$$

$D(E)$ is easy to calculate because H_{int} is short range; nonzero only at the two interfaces between the oligomer and the metal. The nonzero elements of H_{int} form two 2×2 submatrices,

$$H_{\mathrm{int}} = \begin{pmatrix} 0 & -t_1 & 0 & 0 \\ -t_1 & 0 & 0 & 0 \\ 0 & 0 & 0 & -t_1 \\ 0 & 0 & -t_1 & 0 \end{pmatrix}. \tag{16}$$

We have two interface couplings between the metals and the oligomer $H_{\mathrm{int}} = H^L_{\mathrm{int}} + H^R_{\mathrm{int}}$. There is no correlation between these two couplings, so we have

$$\det[1 - \tilde{\mathcal{G}}^0(E) H_{\mathrm{int}}] = \det[1 - \tilde{\mathcal{G}}^0(E) H^L_{\mathrm{int}}] \det[1 - \tilde{\mathcal{G}}^0(E) H^R_{\mathrm{int}}] \equiv D_1(E) D_2(E). \tag{17}$$

Thus we can separate the contribution to $\delta\mathcal{E}$ from the two interface couplings

$$\delta\mathcal{E} = \delta\mathcal{E}^L + \delta\mathcal{E}^R, \tag{18}$$

where

$$\delta\mathcal{E}^L = -\frac{2}{\pi} E \, \mathrm{Im} \ln D_1(E)\Big|_{-2t_0+V_1}^{E_F^L} + \frac{2}{\pi}\int_{-2t_0+V_1}^{E_F^L} \mathrm{Im} \ln D_1(E) dE, \tag{19}$$

$$\delta\mathcal{E}^R = -\frac{2}{\pi} E \, \mathrm{Im} \ln D_2(E)\Big|_{-2t_0+V_2}^{E_F^R} + \frac{2}{\pi}\int_{-2t_0+V_2}^{E_F^R} \mathrm{Im} \ln D_2(E) dE, \tag{20}$$

and where E_F^L (E_F^R) is the Fermi energy of the left (right) metal and

$$D_1(E) = \ln[1 - t_1^2 \tilde{G}^0_{00}(E) \tilde{G}^0_{11}(E)], \tag{21}$$

$$D_2(E) = \ln[1 - t_1^2 \tilde{G}^0_{NN}(E) \tilde{G}^0_{N+1N+1}(E)]. \tag{22}$$

Here the Green's functions for the metals are

$$\tilde{G}^0_{00}(E) = \frac{-i}{\sqrt{4t_0^2 - (E-V_1)^2}} \left[2 - \frac{(E-V_1)^2}{2t_0^2} + i \frac{(E-V_1)}{2t_0^2} \sqrt{4t_0^2 - (E-V_1)^2} \right], \tag{23}$$

$$\tilde{G}^0_{N+1N+1}(E) = \frac{-i}{\sqrt{4t_0^2 - (E-V_2)^2}} \left[2 - \frac{(E-V_2)^2}{2t_0^2} + i \frac{(E-V_2)}{2t_0^2} \sqrt{4t_0^2 - (E-V_2)^2} \right]. \tag{24}$$

The short range of H_{int} enables us to treat it rigorously rather than perturbatively. We included all orders of the interaction t_1.

When the band bottom of the metals is below the lowest level in the oligomer, the interface coupling will not introduce any new localized states because, in this case, $D(E)$ is always positive and there is no solution that satisfies $D(E) = 0$.

The ground-state configuration of the oligomer is determined by

$$\frac{\delta\langle H\rangle}{\delta u_l} = \frac{\delta\langle H_{\mathrm{oli}}\rangle}{\delta u_l} + \frac{\delta\mathcal{E}}{\delta u_l} = 0. \tag{25}$$

When the oligomer is attached to the metals, the lattice configuration will deviate from its isolated one.

We introduce an incoming wave packet, which is taken to have a Gaussian profile,

$$\psi_l(\tau_0) = C \exp\left[i k_0 (l - l_0) - \frac{(l-l_0)^2}{4(\delta l)^2} \right], \tag{26}$$

where k_0 is the average wave number of the wave packet, l_0 its center location, δl its width, and C the normalization constant. To study the dynamics of this incoming wave packet, we solve the time-dependent Schrödinger equation:

$$\left[i\hbar \frac{\partial}{\partial \tau} - H_0(\tau) \right] \psi(\tau) = H_{\rm int} \psi(\tau). \tag{27}$$

Here H_0 implicitly depends on time through the lattice configuration of the oligomer, which evolves after the electron impacts the left interface. We use the Green's function to update the wave function of the incoming wave packet. The Green's function of H_0 at time τ is

$$G^0_{ll'}(\delta\tau;\tau) \equiv -i\langle l| e^{iH_0(\tau)\delta\tau} |l'\rangle = \frac{1}{2\pi}\int_{-\infty}^{\infty} dE \tilde{G}^0_{ll'}(E;\tau) e^{-iE\delta\tau/\hbar}, \tag{28}$$

where $\tilde{G}^0_{ll'}(E;\tau)$ is the Green's function of H_0 at time τ in the energy space which can be calculated from Eq. (9). Thus for the left metal,

$$G^0_{ll'}(\delta\tau;\tau) = (-i) e^{-iV_1\delta\tau/\hbar} [i^{|l-l'|} J_{|l-l'|}(2\delta\tau t_0/\hbar) - i^{|l+l'-2|} J_{|l+l'-2|}(2\delta\tau t_0/\hbar)], \tag{29}$$

and for the right metal

$$G^0_{ll'}(\delta\tau;\tau) = (-i) e^{-iV_2\delta\tau/\hbar} [i^{|l-l'|} J_{|l-l'|}(2\delta\tau t_0/\hbar) - i^{|l+l'-2N|} J_{|l+l'-2N|}(2\delta\tau t_0/\hbar)], \tag{30}$$

where J_l is the lth Bessel function of the first kind, and in the oligomer

$$G^0_{ll'}(\delta\tau;\tau) = -i\sum_i \langle l|\phi_i(\tau)\rangle\langle\phi_i(\tau)|l'\rangle e^{-iE_i\delta\tau/\hbar}. \tag{31}$$

The updated wave function of the incoming wave packet after a small time interval[29] $\delta\tau$ is obtained through the evolution equation

$$\psi_l(\tau+\delta\tau) = i\sum_{l'} G^0_{ll'}(\delta\tau;\tau)\psi_{l'}(\tau) + \frac{1}{\hbar}\int_0^{\delta\tau} d\tau' \sum_{l'l''} G^0_{ll'}(\tau';\tau) H^{l'l''}_{\rm int} \psi_{l''}(\tau). \tag{32}$$

Defining

$$S_{ll'}(\delta\tau;\tau) = \int_0^{\delta\tau} d\tau' G^0_{ll'}(\delta\tau-\tau';\tau), \tag{33}$$

we have

$$\psi_l(\tau+\delta\tau) = i\sum_{l'} G^0_{ll'}(\delta\tau;\tau)\psi_{l'}(\tau) + \sum_{l'l''} S_{ll'}(\delta\tau;\tau) H^{l'l''}_{\rm int} \psi_{l''}(\tau). \tag{34}$$

In the above equations, the scattering potential is short range and therefore the evolution equation contains only one summation. Thus our Green's function approach is efficient for studying the dynamics of transport in organic devices. Our formalism is also easy to extend to other metal and oligomer structures by substituting the appropriate Green's function in the present formula.

Due to the strong electron-lattice coupling in the oligomer, when the incoming wave packet is passing through the oligomer, the lattice will be distorted from its equilibrium position and this distortion in turn changes the electronic structure in the oligomer. Thus we must determine the lattice and the wave packet motion self-consistently. The lattice motion is calculated from the classical equation

$$M\frac{d^2u_l}{d\tau^2} = F_l(\tau) \equiv -\frac{\delta\langle H(\tau)\rangle}{\delta u_l}, \tag{35}$$

where $\delta\langle H(\tau)\rangle/\delta u_l$ consists of the contribution from both $\delta\langle H_{\rm oli}(\tau)\rangle/\delta u_l$ and $\delta\mathcal{E}(\tau)/\delta u_l$. Now $\delta\langle H_{\rm oli}(\tau)\rangle$ contains contributions from both the valence electrons and the incoming wave packet.

The updated lattice configuration and momentum after a small interval $\delta\tau$ is obtained by integrating Eq. (35) over time,

$$u_l(\tau+\delta\tau) = u_l(\tau) + \frac{p_l(\tau)}{M}\delta\tau, \tag{36}$$

$$p_l(\tau+\delta\tau) = p_l(\tau) + F_l(\tau)\delta\tau. \tag{37}$$

To describe the dynamics of the wave packet tunneling through the organic polymer, it is useful to examine the time-dependent energy of the wave packet and of the lattice. It is also useful to analyze the time-dependent energy distribution of the wave packet. From this analysis, we can understand how the energy is exchanged between the incoming wave packet and the lattice dynamically. The energy in the oligomer is the summation of the lattice kinetic and elastic energies and the energies of valence electrons. Before the wave packet impacts the interface, the lattice stays in its equilibrium position and both the lattice kinetic and elastic energy are zero. If we denote the energy change due to the interface couplings in the ground state by $\delta\mathcal{E}_0$ initially, the energy in the lattice at time τ is calculated from

$$E_{\rm latt}(\tau) = \sum_{l=2}^{N-1}\frac{p_l^2(\tau)}{2M} + \frac{K}{2}\sum_{l=1}^{N-1}\Delta_l^2(\tau) + \sum_{i=1}^{N/2}[2E_i(\tau) - 2E_i^0] + [\delta\mathcal{E}(\tau) - \delta\mathcal{E}_0]. \tag{38}$$

Here, $E_i(\tau)$ is the ith eigenvalue of the oligomer electronic Hamiltonian at time τ and E_i^0 the eigenvalue for the initial condition. The expectation value of the energy of the wave packet with the normalized wave function $\psi(\tau)$ at time τ is obtained from

$$E_{\rm wav}(\tau) = \langle\psi(\tau)|H^e|\psi(\tau)\rangle, \tag{39}$$

where $H^e = H^L_{\rm met} + H^R_{\rm met} + H_{\rm oli} + H_{\rm int}$ is the total electronic Hamiltonian.

The total energy of the system which includes the wave packet, all valence electrons, and the lattice elastic and kinetic contributions can be written as

$$E(\tau)=\langle\psi(\tau)|H^e|\psi(\tau)\rangle+\sum_i\langle\phi_i|H^e|\phi_i\rangle+H_{ela}$$

$$+\frac{1}{2}M\sum_l \dot{u}_l^2. \tag{40}$$

Here $H_{ela}\equiv K/2\Sigma_l\Delta_l^2$ is the lattice elastic energy. Since $\psi(\tau)$ satisfies the time-dependent Schrödinger equation, by using the Feynman-Hellman theorem, the time-derivative of the energy is

$$\frac{dE}{d\tau}=\langle\psi(\tau)|\frac{dH^e}{d\tau}|\psi(\tau)\rangle+\sum_i\langle\phi_i|\frac{dH^e}{d\tau}|\phi_i\rangle+\frac{dH_{ela}}{d\tau}$$

$$+M\sum_l\frac{du_l}{d\tau}\frac{d^2u_l}{d\tau^2}. \tag{41}$$

Since the Hamiltonian only depends on τ implicitly through u_l, we have

$$\frac{dE}{d\tau}=\sum_l\frac{du_l}{d\tau}\left[M\frac{d^2u_l}{d\tau^2}+\langle\psi(\tau)|\frac{dH^e}{du_l}|\psi(\tau)\rangle\right.$$

$$\left.+\sum_i\langle\phi_i|\frac{dH^e}{du_l}|\phi_i\rangle+\frac{dH_{ela}}{du_l}\right]. \tag{42}$$

The summation of the last three terms in the above equation is simply $-F_l(\tau)$. Thus the total energy of the system is conserved.

Since the electronic spectrum in our system is continuous, the wave packet has a continuous energy distribution, which is also a function of time. The time-dependent energy distribution of the wave packet is

$$d(E;\tau)=\sum_i|\langle\phi_i|\psi(\tau)\rangle|^2\delta(E-E_i). \tag{43}$$

Here ϕ_i is the eigenfunction of the total electronic Hamiltonian and E_i is the corresponding eigenvalue. We can calculate $d(E;\tau)$ from the Green's functions

$$d(E;\tau)=-\frac{1}{\pi}\mathrm{Im}\sum_i\langle\psi(\tau)|\phi_i\rangle\frac{1}{E-E_i+i0^+}\langle\phi_i|\psi(\tau)\rangle$$

$$=-\frac{1}{\pi}\mathrm{Im}\langle\psi(\tau)|\frac{1}{E-H+i0^+}|\psi(\tau)\rangle$$

$$=-\frac{1}{\pi}\mathrm{Im}\sum_{ll'}\psi_l^*(\tau)\psi_{l'}(\tau)\tilde{G}_{ll'}(E), \tag{44}$$

where $\tilde{G}_{ll'}$ is the Green's function of the electronic Hamiltonian in real space $\tilde{G}_{ll'}(E)=\langle l|(E-H+i0^+)^{-1}|l'\rangle$, which, in our case, can be calculated exactly because of the short range of H_{int}

$$\tilde{\mathcal{G}}(E)=\tilde{\mathcal{G}}^0(E)+\tilde{\mathcal{G}}^0(E)\mathcal{T}(E)\tilde{\mathcal{G}}^0(E), \tag{45}$$

where

$$\mathcal{T}(E)=H_{\mathrm{int}}[1-\tilde{\mathcal{G}}^0(E)H_{\mathrm{int}}]^{-1}. \tag{46}$$

The transmission and reflection coefficients can be obtained by integrating the current over time. The current in the metal is defined as

$$j_l=it_0(\psi_{l+1}^*\psi_l-\psi_l^*\psi_{l+1}), \tag{47}$$

and the coefficients for the normalized incoming wave packet are

$$T=\int_{\tau_0}^{\infty}d\tau j^R(\tau);R=\int_{\tau_0}^{\infty}d\tau j^L(\tau), \tag{48}$$

where we use currents far from the metal/oligomer interfaces,

$$j^L(\tau)=it_0(\psi_l^*\psi_{l+1}-\psi_{l+1}^*\psi_l),\quad l\ll 0, \tag{49}$$

$$j^R(\tau)=it_0(\psi_{l+1}^*\psi_l-\psi_l^*\psi_{l+1}),\quad l\gg N. \tag{50}$$

III. RESULTS

A. Wave-packet evolution and transmission

We present results of our dynamical study using the Green's function formalism. We fix the electronic parameters of the metal and the oligomer and vary the lattice vibration frequency by changing the mass of the oligomer atoms. The electronic parameters of the oligomer are: $\alpha=7$ eV/Å, $K=40$ eV/Å^2, $t_0=2.6$ eV, $t=2.5$ eV, and $t_1=1.5$ eV, which are typical parameters in conjugated polymers.[15] Because the molecules used for molecular wires are also conjugated, these parameters should be also be reasonable for describing these systems. The vibration frequency $\omega=2\sqrt{K/M}$ is tuned by changing the mass M of the oligomer atom. Using a value of M corresponding to trans-polyacetylene gives $\omega=\omega_0=0.22$ eV. We present results for an eight atom oligomer, $N=8$. Figures 2 and 3 are snapshots of the incoming wave packet at different times. Figure 2 is for a small transmission (off-resonance) case and Fig. 3 is for a high transmission (resonance) case. Before the wave packet enters the oligomer, the wave packet has a Gaussian profile. While the wave packet is in the oligomer, the wave-packet profile is severely distorted due to the scattering by the interface and the oligomer. Eventually part of the wave packet is reflected and part is transmitted, and the profile of the wave packet splits into several subwave packets.

From our dynamical calculations, we can determine the time duration over which the wave packet stays in the oligomer (dwell time). In Fig. 4, we plot the total charge density in the oligomer as a function of time. We find that when the energy of the wave packet coincides with that of the discrete energy levels in the oligomer, the wave packet stays in the oligomer for a much longer time than the wave packet with other energies.

Figure 5 describes the transmission as a function of the energy of the incoming electron. The dashed line is the static case, i.e., the oligomer atoms are fixed at their equilibrium positions. The peaks in the transmission spectrum correspond to the discrete energy levels in the oligomer. The first peak indicates the lowest unoccupied level in the oligomer. For finite vibration frequencies, because of the electron-lattice coupling, the lattice will move away from its equilibrium position after the electron wave packet impacts the in-

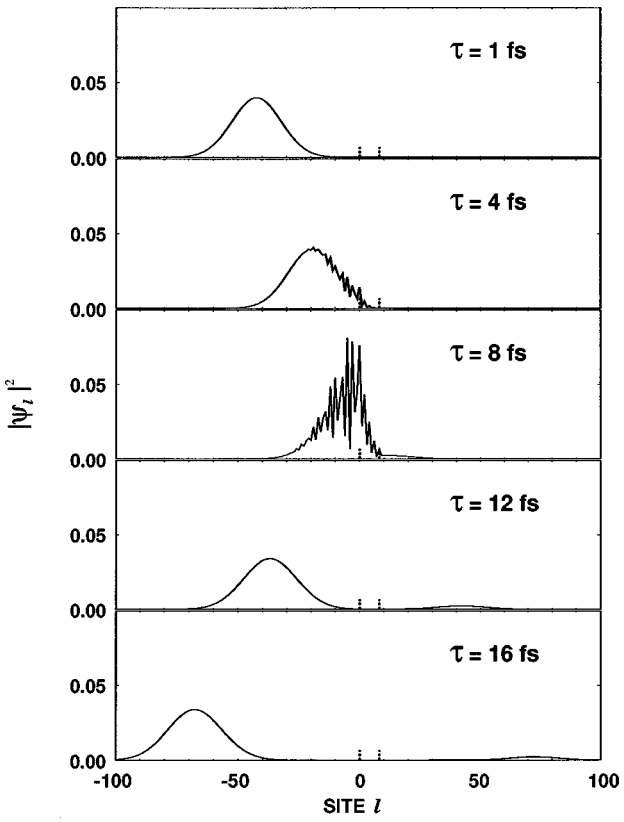

FIG. 2. Snapshots of the wave packet at different times for a small (off-resonant) transmission case ($E=1.2$ eV). The five panels correspond to $\tau=1,4,8,12$, and 16 fs, respectively. The oligomer is between the two dashed lines. The lattice vibration frequency is ω_0.

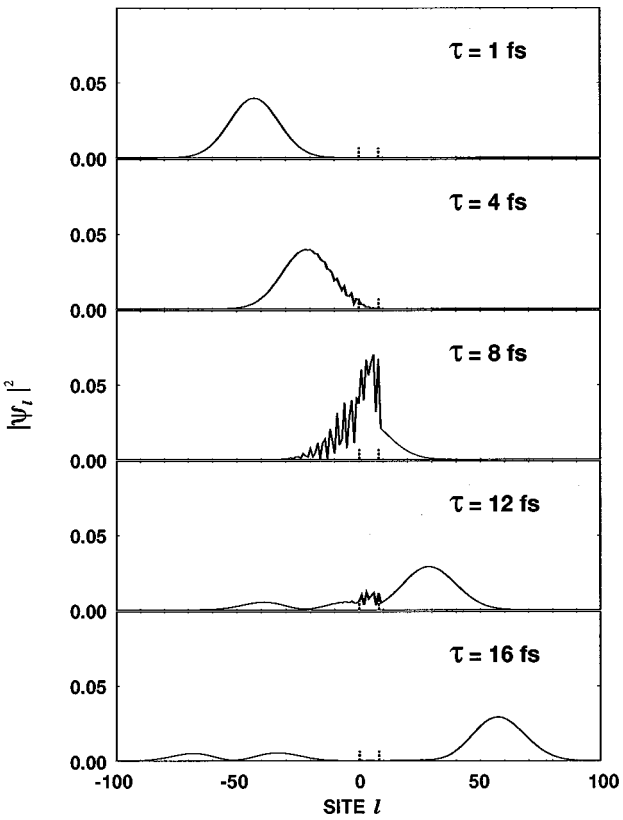

FIG. 3. Snapshots of the wave packet at different times for a large (resonant) transmission case ($E=2.2$ eV). Other parameters and symbols are the same as in Fig. 2.

terface between the oligomer and the metal. The solid line is for the case of $\omega=\omega_0$. We find that the transmission is similar to that of the static case. For the case $\omega=10\omega_0$, as illustrated by the dot-dashed lines, the transmission is dramatically different from that of the $\omega=\omega_0$ case, especially below the conduction-band edge. The first transmission peak shifts toward lower energy, which indicates some subgap electron levels.

In inorganic double barrier tunneling structures, phonon-assisted tunneling and phonon side peaks in the transmission spectrum have been observed.[18–20] In the organic-based devices, since the lattice is described classically, the energy in the lattice is not quantized and we do not observe the phonon side peaks. However, because the self-trapped polaron may be formed, which is below the conduction-band edge, we can observe that the peak in transmission shifts toward the polaron level.

To more clearly illustrate the different transmission behavior for the different lattice vibrational frequencies, we examined the evolution of the wave function of the incoming wave packet and the lattice configuration. We calculate the charge density of the incoming electron and the lattice configuration in the oligomer for different time to study the correlation between the electronic and the lattice motion for these two cases. Figure 6 illustrates the case in the low-frequency regime, $\omega=\omega_0$. The circles, squares, and triangles correspond to $\tau=6$, 8, and 10 fs. Figure 6(a) shows that from 6–10 fs, the wave packet is moving from the left interface to the right one. Because of the electron-lattice coupling, the lattice moves away from its equilibrium configuration as in Fig. 6(b). However, during $t=6$ to $t=10$ fs the lattice motion is within its first vibrational period and lags far behind the incoming electron. Thus the carrier is like a free electron and the transmission is almost the same as that in the static case.

The high-frequency $\omega=10\omega_0$ results are shown in Fig. 7. The lattice behavior is quite different from that for $\omega=\omega_0$. During the period from 6–10 fs, as the wave packet moves from the left interface to the right one, the profile of the lattice distortion also moves through the oligomer, following the wave packet motion. In other words, the carrier in this case is no longer a free electron but rather the electron is surrounded by the lattice distortion, like a self-trapped polaron. This carrier behavior leads to the first transmission peak shifting toward the polaron level in the oligomer, which lies below the energy gap, as shown in Fig. 5.

B. Energy exchange between wave packet and lattice

The transport behavior in various frequency regimes can also be studied by focusing on the evolution of the energy in the wave packet and the energy in the oligomer. Figure 8 depicts the energy of the incoming wave packet and that in the oligomer as a function of time for the case of $\omega=\omega_0$. The energy in the oligomer consists of three parts: lattice kinetic and elastic energy, valence electron energy, and $\delta\mathcal{E}$ due to the interface couplings. In the low-frequency regime, after the wave packet enters the oligomer, the wave packet

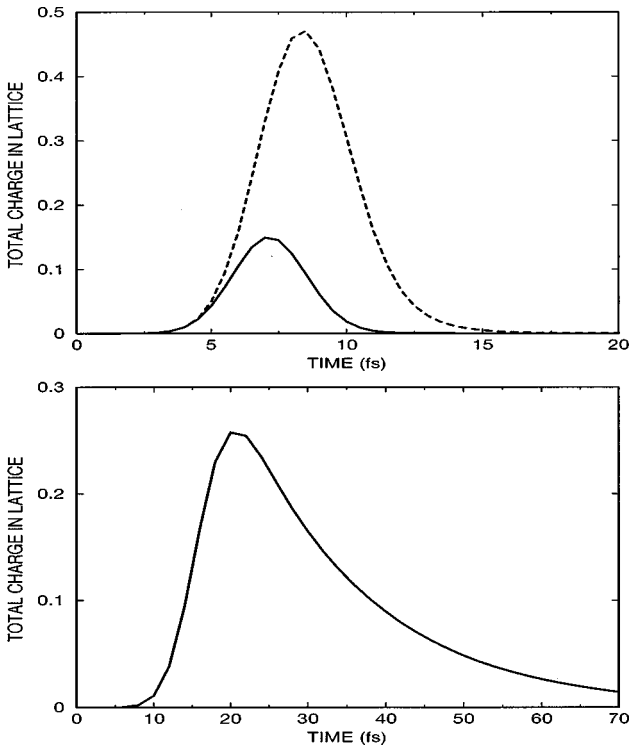

FIG. 4. The total charge density in the oligomer as a function of time. In panel (a), the solid line is for a small (off-resonant) transmission (Fig. 2) and the dashed one is for the large (resonant) transmission (Fig. 3). Parameters are the same as in Fig. 2. In panel (b), the interface coupling is small ($t_1=0.5$ eV) and the width of the initial wave packet is large ($\delta l=20$ lattice constants) so as to manifest the resonant tunneling effects.

loses some energy gradually and at the same time the lattice gains some energy; the total energy of the wave packet and the lattice is conserved. In the lattice, the energy increases monotonically and saturates when the wave packet has passed through the oligomer. This is to be expected since the incoming electron causes the lattice motion when it passes through the oligomer, and in this case the lattice motion lags behind the electron. This lattice motion has no correlation with the electron: the wave packet just excites the lattice

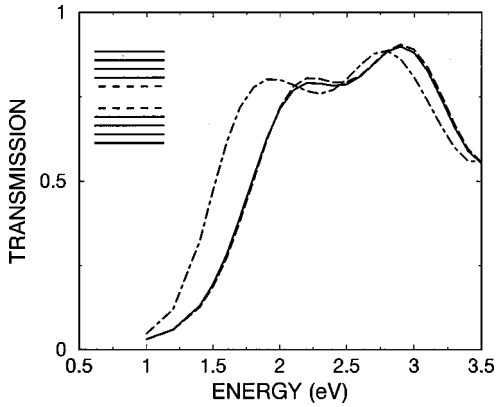

FIG. 5. Electronic transmission as a function of the incoming wave-packet energy for $\alpha=7$ eV/Å. The dashed, solid, and dot-dashed lines correspond to $\omega=0$, $\omega=\omega_0$, and $\omega=10\omega_0$, respectively. The inset shows schematically the electronic levels of the oligomer; dashed lines denote polaron levels.

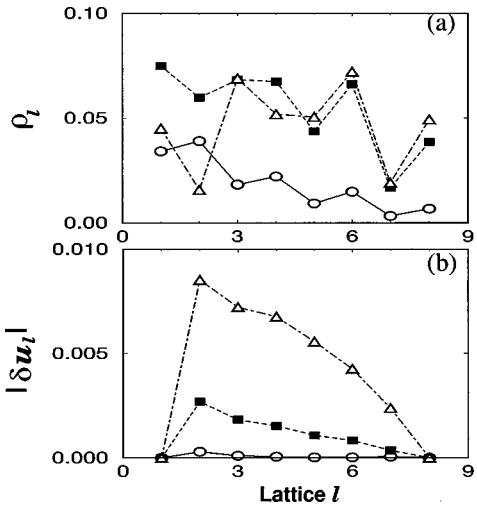

FIG. 6. Snapshot of (a) charge density of the wave packet and (b) magnitude of the lattice distortion in the oligomer for $\omega=\omega_0$. The circles, squares, and triangles correspond to $\tau=6$, 8, and 10 fs. The energy of the incoming wave packet is 2.1 eV.

motion through the electron-lattice coupling, but cannot obtain the feedback from the lattice. Thus the energy in the lattice is monotonic.

In the high-frequency regime, as shown in Fig. 9, the energy in the lattice is localized for some period when the incoming wave packet is in the oligomer, indicating the highly correlated motion between the incoming wave packet and the lattice. Since in this case, the lattice distortion is localized around the wave packet, the peak corresponds to the whole wave packet being in the oligomer, which has the largest lattice distortion and therefore the largest energy exchange in lattice.

To obtain more detailed information about the energy exchange occurring when the wave packet passes through the oligomer, we show in Figs. 10 and 11 the energy distribution of the wave packet for different times. We see that the initial wave packet has a Gaussian distribution around its

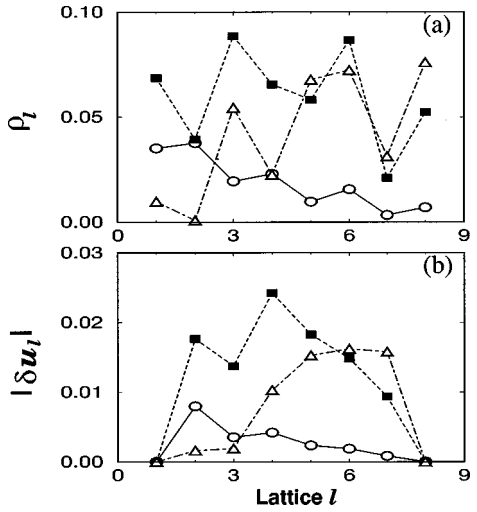

FIG. 7. Snapshot of (a) charge density of the wave packet and (b) magnitude of the lattice distortion in the oligomer for $\omega=10\omega_0$. Symbols and the energy of wave packet are the same as in Fig. 6.

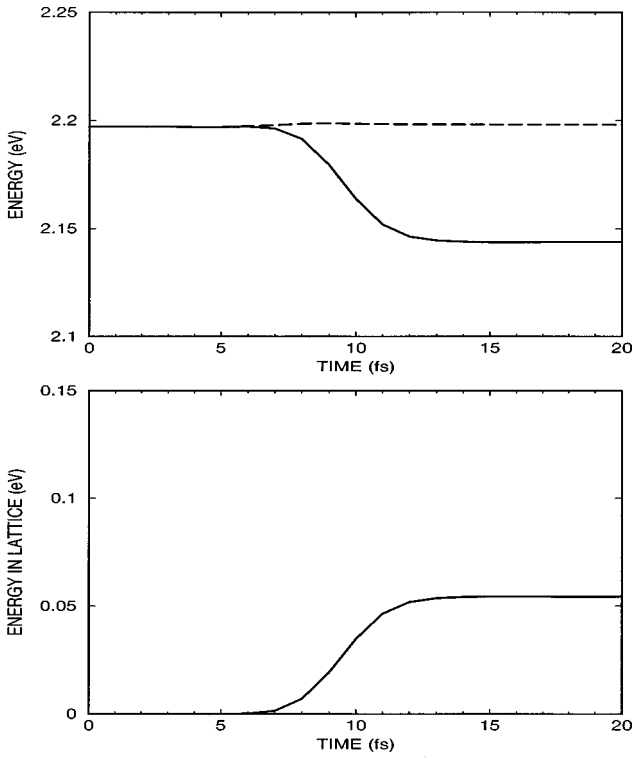

FIG. 8. Energy of the wave packet (a) and the lattice (b) as a function of time for $\omega=\omega_0$. The dashed line in panel (a) is the total energy of the wave packet and the lattice. The energy of the incoming wave packet is $E=2.2$ eV.

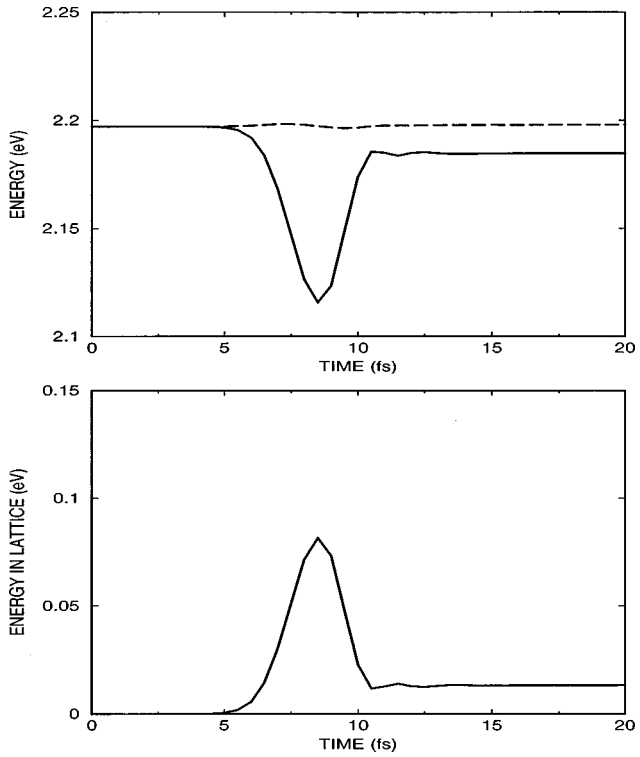

FIG. 9. Energy of the wave packet (a) and the lattice (b) as a function of time for $\omega=10\omega_0$. The symbols and the energy of the wave packet are the same as in Fig. 8.

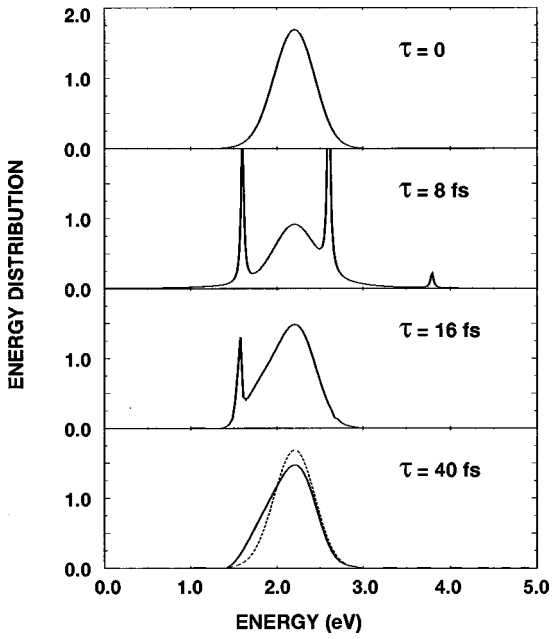

FIG. 10. Energy distribution of the incoming wave packet at different times for $\omega=\omega_0$. Panels (a)–(d) correspond to $\tau=0,8,16,$ and 40 fs, respectively. The dashed line in panel (d) is identical to panel (a) for reference purposes. The energy of the incoming wave packet is $E=2.2$ eV.

average energy. While the wave packet is in the oligomer, the energy distribution changes dramatically with some sharp peaks, which correspond to the discrete levels of the oligomer. Because the wave-packet tail stays in the oligomer for a long time, the peaked structure of the energy distribution is maintained for a long time. Eventually the energy distribution is restored to a smooth one. By comparing the final energy distribution to the initial one, we find different behavior of the wave-packet energy distribution for the two vibra-

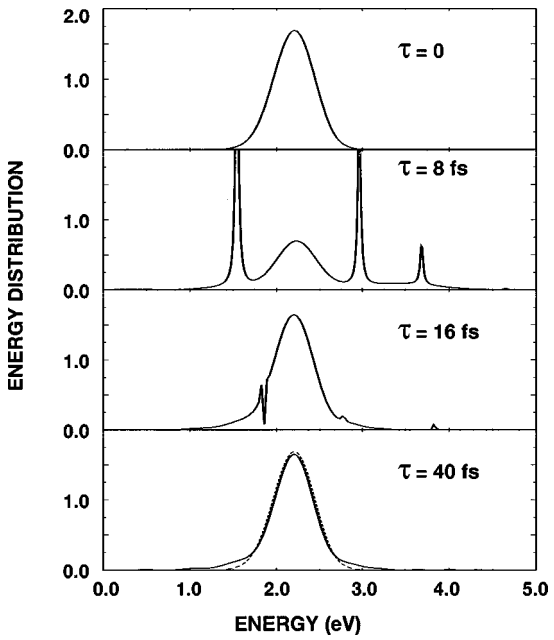

FIG. 11. Energy distribution of the incoming wave packet at different times for $\omega=10\omega_0$. Symbols and the energy of the wave packet are the same as in Fig. 10.

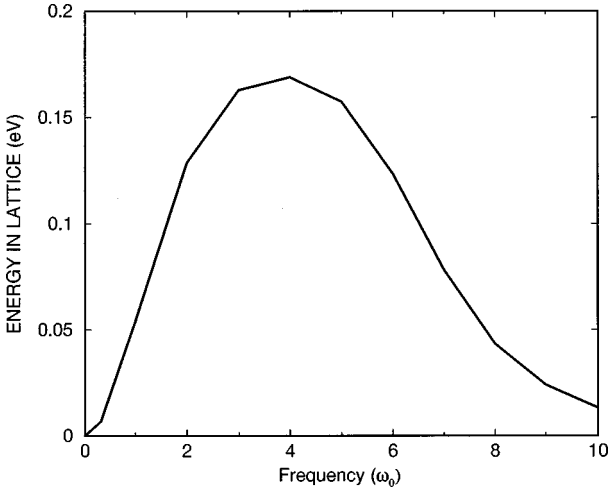

FIG. 12. The energy left in the lattice as a function of the lattice vibrational frequency. The energy of the incoming wave packet is fixed at $E=2.2$ eV.

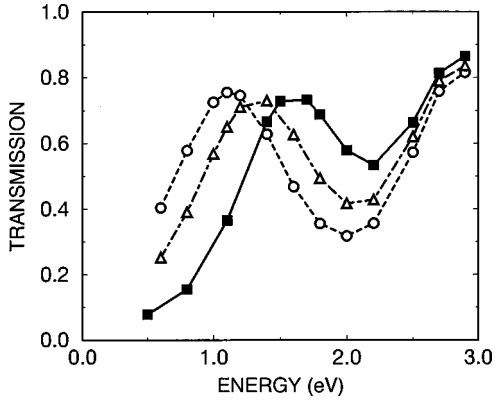

FIG. 13. Electronic transmission as a function of the incoming wave-packet energy with a pre-existing polaronlike lattice distortion. The electron-lattice coupling is $\alpha=5.6$ eV/Å. Dashed and dot-dashed lines correspond to $\omega=0$ and $\omega=\omega_0$. The solid line is for reference purpose, obtained by using the equilibrium lattice configuration and $\omega=\omega_0$.

tional frequencies. In the low-frequency regime ($\omega=\omega_0$), the final distribution becomes asymmetric and the wave packet gains some weight below the distribution peak, although the location of the peak does not change significantly. This result is consistent with the picture that the wave packet loses energy in the lattice and lattice excitations are left behind the wave packet in this regime. In the high-frequency regime, however, the final distribution is nearly symmetric and is simply broadened compared to the initial one. The energy of the final wave packet is nearly the same as that of the initial one. This result is consistent with the picture of highly correlated electron and lattice motion in this regime: after the wave packet has passed through the oligomer, the lattice stays near its equilibrium position and little energy is transferred to the lattice.

The energy left in the lattice after the wave packet has passed through the oligomer depends on the phonon frequency. We plot in Fig. 12 the energy left in the lattice as a function of the phonon frequency of the oligomer. We see that in both low- and high-frequency limits, the energy in the lattice approaches zero. This is expected because, in the low-frequency limit, the lattice cannot move and the lattice cannot be excited; whereas in the high-frequency limit, the motion of the electron and lattice are highly correlated and after the wave packet has passed through the oligomer, the lattice stays near its equilibrium position and little energy is transferred to the lattice. The difference between these two limits is that in the high-frequency limit, the energy in the lattice changes with time when the wave packet is moving through the oligomer.

We also find a similar crossover behavior for a fixed vibrational frequency $\omega=\omega_0$ by tuning the electronic time scale. The electronic scale is determined by its momentum. In the one-dimensional tight-binding model of the metal, the dispersion is $E=V_1-2t_0\cos k$ and the time scale is $\hbar/|2t_0\sin k|$. Thus for an incoming electron with a fixed energy, we can change V_1 to obtain different momenta of the electron. Thus whether the carrier is like a free electron or a polaron depends on the ratio between the electron time scale and the lattice time scale.

C. Lattice fluctuation effects: a preexisting polaron

Strong lattice fluctuations may significantly influence electronic transmission through the organic segment. Due to the low dimensionality of polymers, lattice fluctuations can be sufficiently strong to produce some transient solitonlike or polaronlike lattice distortion.[30,31] Since the polaron configuration has the most important contribution to lattice fluctuations in oligomers, we consider a preexisting polaron lattice distortion and calculate the wave-packet transmission to study fluctuation effects. In Fig. 13, we show the transmission as a function of the energy of the incoming wave packet with a preexisting polaronlike lattice distortion. The dashed and dot-dashed lines correspond to $\omega=0$ and $\omega=\omega_0$. For $\omega=0$, because the lattice does not move, the first resonant tunneling peak is from the polaron level in the oligomer. For $\omega=\omega_0$, although the first transmission peak shifts from the polaron level toward higher energy compared to the case of $\omega=0$, it is still much lower than the energy gap (first peak of the solid line). This indicates that the wave packet can use a ''partially formed'' polaron level produced by lattice fluctuations to tunnel through the oligomer, although the carrier behavior here is more like a free electron. Thus polaron effects may be important even in the low-frequency regime due to the presence of strong lattice fluctuations in oligomers. The present realization of lattice fluctuations is more realistic compared to the previous approximation treated as static disorder.[14] The subgap transmission is enhanced in both cases, although at somewhat different energies.

IV. SUMMARY AND CONCLUSION

In this paper, we have studied the dynamics of charge transport in metal/organic/metal tunneling structures. We have introduced a model which consists of two semi-infinite metal contacts attached to the polymer chain. Conjugated organic materials are quite different from inorganic semiconductors in that the lattice in organics is flexible and readily distorted and there is a strong electron-lattice coupling. To understand the transport in these devices, it is necessary to solve both the electronic and lattice motions self-

consistently. Existing dynamical approaches used for finite homogeneous polymer models are not suitable to study these organic tunneling structures. To this end, we developed a physically intuitive and numerically efficient Green's function approach to investigate the dynamics of transport in organic-based devices. In this formalism, we have treated the coupling between the oligomer and metals as the interaction. The short range of this interaction enabled us to treat it rigorously rather than perturbatively and to study the dynamics very efficiently. The formalism is readily extended to other organic structures where a dynamical study would also be appropriate.

The transport behavior in the metal/organic/metal structures depends on the ratio between the electronic and lattice time scales. For fixed electronic structure, by increasing the lattice vibrational frequency, the carrier behavior changes from free-electron-like to polaronlike. In the former, the lattice motion lags behind the incoming wave packet and the transmission is very close to that in the rigid-lattice case. In contrast, in the latter case, the lattice follows the electron, forming a lattice distortion cloud, and the first transmission peak shifts from the conduction-band edge to the self-trapped polaron level. We also observed this crossover for a fixed lattice vibrational frequency by tuning the velocity of the incoming wave packet. We have investigated the transmission properties, the transfer of energy between the incident electron and the oligomer, and the time evolution of the electron energy distribution, as the ratio of these time scales is changed. We have calculated the dynamical electronic transmission with a preexisting lattice distortion to simulate lattice fluctuations. Strong lattice fluctuations in one-dimensional oligomers may lead to transient polaronlike lattice distortions, which change the transmission of these tunnel structures substantially even in the low phonon frequency regime. Our microscopic results should provide valuable input to macroscopic device models, e.g., cross sections for scattering events and carrier mobilities.

ACKNOWLEDGMENTS

This work was supported by the LDRD program on Molecularly Engineered Electronics Materials at LANL and the U.S. Department of Energy.

[1] See, e.g., J.H. Burroughes *et al.*, Nature (London) **347**, 539 (1990).
[2] P.L. Burn *et al.*, Nature (London) **347** 539 (1990).
[3] G. Gustaffson *et al.*, Nature (London) **357**, 477 (1992).
[4] L.A. Bumm *et al.*, Science **272**, 1323 (1996).
[5] I.H. Campbell *et al.*, Phys. Rev. B **54**, R14 321 (1996).
[6] F. Nuesch *et al.*, Adv. Mater. **9**, 222 (1997).
[7] R.P. Andres *et al.*, Science **273**, 1690 (1996).
[8] S. Datta *et al.*, Phys. Rev. Lett. **79**, 2530 (1997); W.D. Tian *et al.*, J. Chem. Phys. **109**, 2874 (1998).
[9] C. Boulas *et al.*, Phys. Rev. Lett. **76**, 4797 (1996).
[10] A. Yazdani *et al.*, Science **272**, 1921 (1996).
[11] C. Joachim and J.F. Vinuesa, Europhys. Lett. **33**, 635 (1996).
[12] S. Datta and W. Tian, Phys. Rev. B **55**, R1914 (1997).
[13] M.P. Samanta *et al.*, Phys. Rev. B **53**, R7626 (1996).
[14] Z.G. Yu *et al.*, Phys. Rev. B **56**, 6494 (1997); J. Phys.: Condens. Matter **10**, 617 (1998).
[15] A.J. Heeger *et al.*, Rev. Mod. Phys. **60**, 781 (1988).
[16] A. Kadyshevitch and R. Naaman, Surf. Interface Anal. **25**, 71 (1997); Phys. Rev. Lett. **74**, 3443 (1995).
[17] A. Haran *et al.*, Chem. Phys. Lett. **268**, 475 (1997).
[18] F.F. Ouali *et al.*, Phys. Rev. Lett. **75**, 308 (1995).
[19] C. Zhang *et al.*, Phys. Rev. Lett. **72**, 3397 (1994).
[20] W. Cai *et al.*, Phys. Rev. Lett. **65**, 104 (1990).
[21] F. Rossi, A.D. Carlo, and P. Lugli, Phys. Rev. Lett. **80**, 3348 (1998).
[22] Y. Ono and A. Terai, J. Phys. Soc. Jpn. **59**, 2893 (1990).
[23] M. Kuwabara, Y. Ono, and A. Terai, J. Phys. Soc. Jpn. **60**, 1286 (1991); Y. Ono, M. Kuwabara, and A. Terai, *ibid.* **60**, 3120 (1991); M. Kuwabara, Y. Ono, and A. Terai, *ibid.* **61**, 2412 (1992).
[24] M. Kuwabara, A. Terai, and Y. Ono, J. Phys. Soc. Jpn. **65**, 992 (1996).
[25] Y. Arikabe, M. Kuwabara, and Y. Ono, J. Phys. Soc. Jpn. **65**, 1317 (1996).
[26] M. Kinoshita, Y. Hirano, M. Kuwabara, and Y. Ono, J. Phys. Soc. Jpn. **66**, 703 (1997).
[27] A. Yamashiro and A. Takahashi, J. Phys. Soc. Jpn. **67**, 2938 (1998).
[28] See, e.g., J. Callaway, *Quantum Theory of the Solid State*, 2nd ed. (Academic Press, San Diego, 1991).
[29] We use a very small $\delta\tau$ (0.01 fs) in our calculations to ensure reliable results.
[30] R.H. McKenzie and J.W. Wilkins, Phys. Rev. Lett. **71**, 4015 (1993).
[31] F.H. Long *et al.*, Phys. Rev. Lett. **71**, 762 (1993).